Investigation of the Electrochemical Properties of CoAl-Layered Double Hydroxide/Ni(OH)$_2$

Hui Li,[1] F. Musharavati,[2] Jingtao Sun,[1] Fadi Jaber,[3] Erfan Zalnezhad,[1,z] K. N. Hui,[4,z] and K. S. Hui[5,z]

[1]*Department of Mechanical Convergence Engineering, Hanyang University, Seongdong-gu, Seoul 04763, Korea*
[2]*Mechanical and Industrial Engineering Department, College of Engineering, Qatar University, 2713 Doha, Qatar*
[3]*Department of Biomedical Engineering, Ajman University, Ajman, United Arab Emirates*
[4]*Institute of Applied Physics and Materials Engineering, University of Macau, Macau, People's Republic of China*
[5]*School of Mathematics, University of East Anglia, Norwich NR4 7TJ, United Kingdom*

Layered double hydroxides (LDH) as active electrode materials have become the focus of research in energy storage applications. The manufacturing of excellent electrochemical performance of the LDH electrode is still a challenge. In this paper, the production of CoAl-LDH@Ni(OH)$_2$ is carried out in two steps, including hydrothermal and electrodeposition techniques. The prominent features of this electrode material are shown in the structural and morphological aspects, and the electrochemical properties are investigated by improving the conductivity and cycle stability. The core of this experimental study is to investigate the properties of the materials by depositing different amounts of nickel hydroxide and changing the loading of the active materials. The experimental results show that the specific capacity is 1810.5F · g^{-1} at 2 A/g current density and the cycle stability remained at 76% at 30 A g^{-1} for 3000 cycles. Moreover, a solid-state asymmetric supercapacitor with CoAl-LDH@Ni(OH)$_2$ as the positive electrode and multi-walled carbon nanotube coated on the nickel foam as the negative electrode delivers high energy density (16.72 Wh kg^{-1} at the power density of 350.01 W kg^{-1}). This study indicates the advantages of the design and synthesis of layered double hydroxides, a composite with excellent electrochemical properties that has potential applications in energy storage.

Supercapacitors (SCs) are currently of widespread interest in energy storage, which has become a research area due to the development of various energy storage devices, long cycle life, high power density, high safety, and low maintenance costs. Numerous studies have concentrated on the enhancing the performance of the electrode material. Electrochemical capacitors (ECs), also known as supercapacitors,[1,2] are a new type of energy storage device that have been developed in recent years. Typically, according to the charge storage mechanism of different electrode materials,[3–5] the use of supercapacitors can be divided into two categories including the electric double layer capacitor (EDLC), Faraday pseudocapacitor and hybrid supercapacitor.[6–9] The electric double layer capacitor uses high surface area carbon as the electrode material, while the Faraday pseudocapacitor uses a transition metal oxide or a conductive polymer as an electrode material.

The electric double layer capacitor is a new capacitor which is based on the interface of the double layer theory.[10,11] The reversible electrostatic adsorption /desorption on the electrode surface is used to store the charge.[12] By arrangement of the opposite sign charge an electric double layer is formed in the vicinity of the electrode/electrolyte interface, a so-called "electric double layer capacitor".[13,14] Its working principle is: the electrode surface and solution on both sides of the electrolyte solution appear on the opposite sides of the excess charge.

Hydrotalcite-like layered clays, also well-known LDH,[15–18] have been extensively explored in the field of catalysts and catalyst supports,[19] flame retardants,[20] anion exchange,[21] optical and electrical functional materials,[22] and Nano-additives. LDH are rich in lamellae as electrode materials for supercapacitors. On one hand, by providing a large specific surface area, its electric double layer capacitance can be improved, and on the other hand, a high degree of redox reaction at the surface of the electrode provides a Faraday quasi-capacitance higher than that of the electric double layer capacitor. Wang et al. (2007)[23] first reported the thin film electrode fabricated from Co/Al nanosheets through drying of a colloidal solution of Co-based LDH nanosheets (an almost transparent solution) on an indium tin oxide deposited on glass. Su et al.[24] described a technique to develop the capacitive properties of Co/Al-LDHs by means of mixing hexacyanoferrate (II) and hexacyanoferrate (III) anion solutions jointly or separately with an aqueous solution of 1 M KOH.[25] LDH have shown great application

prospects in the fields of catalysis, ion exchange, electrochemistry, adsorption, environmental protection, etc. With the development of science and the deepening of research, the preparation method has developed. LDH are mainly prepared by a salt and alkali reaction, salt and oxide reaction, and ion exchange reaction system. Based on the above methods to optimize and improve the main method derived from different methods. These include the coprecipitation method, hydrothermal method, the reconstruction method, and the ion exchange process.[23–32]

In this paper, the composite material of CoAl-LDH was prepared by the hydrothermal method, and the adhesive-free, well-bonded three-dimensional (3D) LDH @Ni(OH)$_2$ composite was built using the electrochemical deposition of the cobalt hydroxide nanosheet on the LDH base, to improve the material electrochemical performance. The performance of the composites was analyzed by cyclic voltammetry, electrochemical impedance spectroscopy, and constant current charging. The structural and morphological characterizations of the composites were analyzed by scanning electron microscopy (SEM), energy dispersive X-ray spectroscopy (EDS), XRD and X-ray photoelectron spectroscopy (XPS).

Experimental

Preparation of Co/Al-LDH composite.—0.582 g Co(NO$_3$)$_2$ · 6H$_2$O (>97%, sigma) and 0.375 g Al(NO$_3$)$_2$ · 9H$_2$O (>97%, sigma) were mixed with 50 mL deionized water in breaker with n(Co)/n(Al) = 2:1, and the mixture sonicated for 1 h. Then, 2.102 g Co(NH$_2$)$_2$ (>97%, sigma) and 0.185 g NH$_4$F (≥99%, sigma) were added to the mixture which were sonicated in a clean beaker for 2 h to obtain a homogeneous suspension. The homogenized suspension was ultrasonically treated and poured into an 80 ml Teflon-lined autoclave. Finally, cleared Nickel Foam (NF) (1 cm × 1 cm) was placed in the autoclave and heated to 120°C for 12 h in an oven. Figure 1a shows the schematic of hydrothermal treatment process.

Ni(OH)$_2$ coating preparation.—The schematic of the electrochemical deposition of CoAl-LDH@NF (1 × 1cm) is shown in Fig. 1b. The electrodeposition was carried out in a standard three-electrode electrochemical workstation (ZIVE SP2, 10 μHz~4 MHz). The CoAl-LDHs@NF, a saturated calomel electrode (SCE), and a

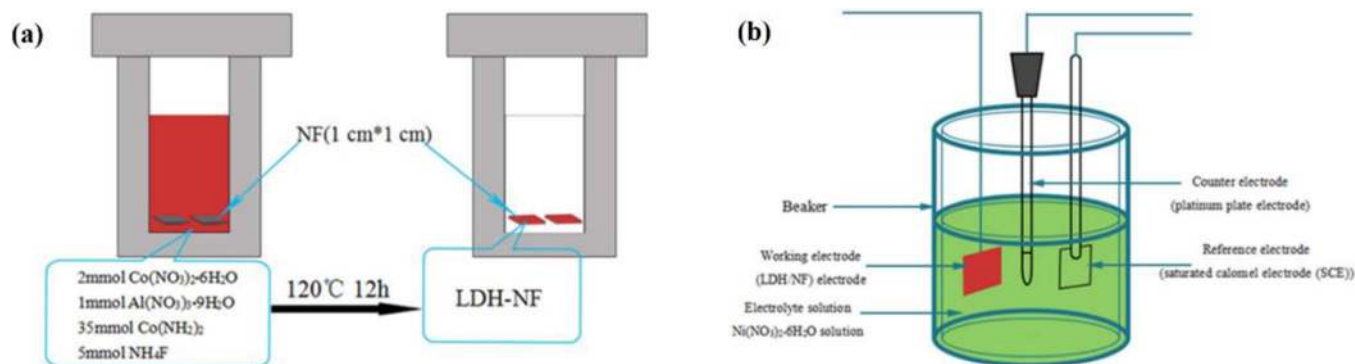^{z}E-mail: erfan@hanyang.ac.kr; bizhui@umac.mo; k.hui@uea.ac.uk

Figure 1. (a) Schematic illustrations of synthesis process for CoAl-LDH composites and (b) CoAl-LDH@Ni(OH)$_2$ composites.

platinum (Pt) plate were selected as the working electrode, reference electrode, and counter electrode, respectively. The experimental process was performed at a scan rate of 5 mV^{-1} for different cycles within a voltage range of −1.1 V to 0.25 V in 6 mM Ni(NO$_3$)$_2$•6H$_2$O solution by the cyclic voltammetric electrodeposition method. The electrodes were deposited with different number of cycles including 4, 6, 8, and 10 cycles and considered as CoAl-LDH@Ni(OH)$_2$-C1, CoAl-LDH@Ni(OH)$_2$-C2, CoAl-LDH@Ni(OH)$_2$-C3, and CoAl-LDH@Ni(OH)$_2$-C4, respectively. Finally, the composite binder free electrodes were washed in distilled water and dried in a vacuum oven for 12 h at 60°C.

Preparation of PVA/KOH electrolyte and MWCNT negative electrode.—3 g of PVA and 3 g of KOH were dissolved in distilled water with agitation at 80°C for 5 h. After complete dissolution, the excess water was evaporated at room temperature and eventually a PVA–KOH gel electrolyte was obtained.

MWCNT (80 wt%), graphite (10 wt%) and Polyvinylidene fluoride (PVDF,10 wt%) were mixed in N-Methyl pyrrolidone (NMP). The resultant mixture was milled and the paste placed in the nickel-foam substrate and dried at 80°C for 6 h.

Electrochemical measurements.—The entire electrochemical performance test was conducted on an electrochemical workstation and was performed at ambient temperature. The obtained electrode, platinum mesh, Hg/HgO electrode, and the 6 mol/L KOH solution were utilized as the working electrode, auxiliary electrode, reference electrode, and the electrolyte, respectively.
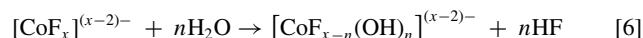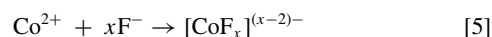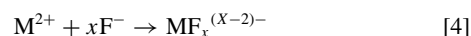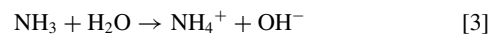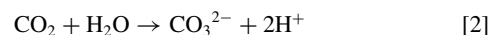
After the deposition process, the Ni(OH)$_2$ on the LDH-NF substrate was rinsed with distilled water and kept in a vacuum oven for 12 h at 60°C. The Ni(OH)$_2$ in the electrode was directly weighed by an electronic microbalance (Mettler Toledo, GB204, d = 0.01/0.1 mg).

After the working electrode was immersed in the electrolyte solution for 3 h, the cyclic voltammetry (CV) and constant current charging and discharging tests were performed using the ZIVE SP2 electrochemical workstation. The CV was tested at a voltage of 0∼0.65 V (Hg/HgO) and a scan rate of 5 mVs^{-1}. The constant current charge and discharge curves of the potential range of 0∼0.6 V (Hg/HgO) were measured at different current densities. A SASC device was assembled using CoAl-LDH @Ni(OH)$_2$@NF as the positive electrode, MWCNT@NF as the negative electrode and the PVA/KOH gel electrolyte between them. The mass loading for the negative electrode was determined by balancing the charges stored in each electrode.

Characterization.—Powder X-ray diffraction (XRD, Rigaku MiniFlex-II desktop, Cu Kα) was performed on the coated samples by Cu Kα radiation (λ = 0.15406 nm) at 40 kV and 30 mA. The scan speed was 5° min-1 with a 0.02°step. The y structure and morphology of the samples were characterized on a field emission scanning electron microscopy (FESEM, LEO-1550) with an applied voltage of 5 kV and energy-dispersive X-ray spectroscopy (EDS).

Results and Discussion

The process of the layered structure of CoAl-LDH@Ni(OH)$_2$ as a binderless electrode generally includes two steps as illustrated schematically in Figure 2. First, through the hydrothermal synthesis technique the CoAl-LDH substrate was obtained. During the hydrothermal process, the metal ions (Co^{2+}, Al^{3+}) reacted with CO$_3^{2-}$ and OH$^-$ (decomposed from urea) to form CoAl-LDH particles that were grown directly on NF as the reaction continued as shown the formula (1–3). And according to the reactions (4,5), the fresh Co parent solution [CoF$_x$]$^{(x-2)-}$ is prepared. Then, in the presence of water, there is a reversible hydrolytic reaction for [CoF$_x$]$^{(x-2)-}$ and [CoF$_{x-n}$(OH)$_n$]$^{(x-2)-}$ producing hydrogen fluoride (6).

$$CO(NH_2)_2 + H_2O \rightarrow 2NH_3 + CO_2 \qquad [1]$$

$$CO_2 + H_2O \rightarrow CO_3^{2-} + 2H^+ \qquad [2]$$

$$NH_3 + H_2O \rightarrow NH_4^+ + OH^- \qquad [3]$$

$$M^{2+} + xF^- \rightarrow MF_x^{(X-2)-} \qquad [4]$$

$$Co^{2+} + xF^- \rightarrow [CoF_x]^{(x-2)-} \qquad [5]$$

$$[CoF_x]^{(x-2)-} + nH_2O \rightarrow \left[CoF_{x-n}(OH)_n\right]^{(x-2)-} + nHF \qquad [6]$$

After that, the CoAl-LDH substrate was placed in Ni(NO$_3$)$_2$•6H$_2$O solution by the cyclic voltammetric electrodeposition method to form CoAl-LDH@Ni(OH)$_2$ with a core-shell structure. The NF substrate

Figure 2. Schematic and SEM illustration of the two steps synthesis of hierarchical CoAl-LDH@Ni(OH)$_2$ electrode.
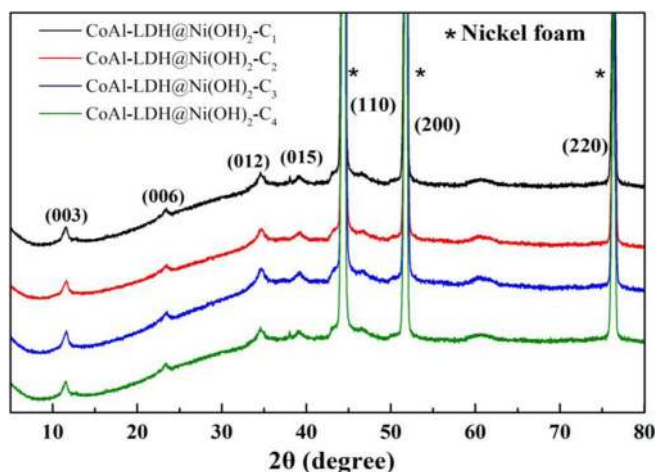
Figure 3. XRD patterns of CoAl-LDH@Ni(OH)$_2$.

was covered by CoAl layer with a core-shell structure during the hydrothermal process. Then, a thin layer of Ni(OH)$_2$ was electrode-posited deposited on the surface of as-prepared LDH. The deposition process of the Ni(OH)$_2$ are as follows (7, 8):

$$NO_3^- + 7H_2O + 8e^- \rightarrow NH_4^+ + 10OH^- \qquad [7]$$

$$Ni^{2+} + 2OH^- \rightarrow Ni(OH)_2 \qquad [8]$$

Figure 3 presents the XRD of CoAl-LDH@Ni(OH)$_2$ obtained by electrodeposition at different cycles numbers (C1, C2, C3, and C4 represent 4, 6, 8, and 10 cycles, respectively). Three typical peaks, marked with asterisks, originate from nickel foam.[26] As can be seen from the figure, the peaks at 11.4°, 22.7°, 34.4°, and 38.8° are in-dexed as (003), (006), (012), and (015), respectively. The diffraction patterns show some characteristic reflections of (003), (006), (012), and (015), showing a symmetry and a typical hydrotalcite-like struc-ture (JCPDS15-0087), indicating that the layered structure was suc-cessfully obtained.[27] In addition, XRD confirmed that Ni(OH)$_2$ was present in CoAl-LDH@Ni(OH)$_2$. Some peaks at 11.4° and 22.7° can be indexed to Ni(OH)$_2$. For CoAl-LDH@Ni(OH)$_2$, because of the different number of electrodeposition, the diffraction peaks and their basal spacing are slightly different. The interlayer spacing depends on the orientation and size of the charge-balancing anion, which reflects the homogeneous orientation of hydrotalcite-like nanosheets that can reduce some typical reflection intensity.

The chemical composition and the surface chemical state of the CoAl-LDH@Ni(OH)$_2$ composites were investigated by X-ray photo-electron spectroscopy (XPS) technique. The XPS survey spectrum of the composite not only Co 2p, Al 2p and O 1s peaks, but also shows the peaks of Ni 2p (Fig. 4a). The Ni 2p and Co 2p XPS spectrum (Figs. 4b and 4c) showed the 2p3/2 and 2p1/2 levels of Ni^{2+} and Co^{2+} distributed in the main peak of 856 eV, 873 eV and 781 eV, 796 eV, respectively. And complement the XPS spectrum of O 1s (Fig. 4d)
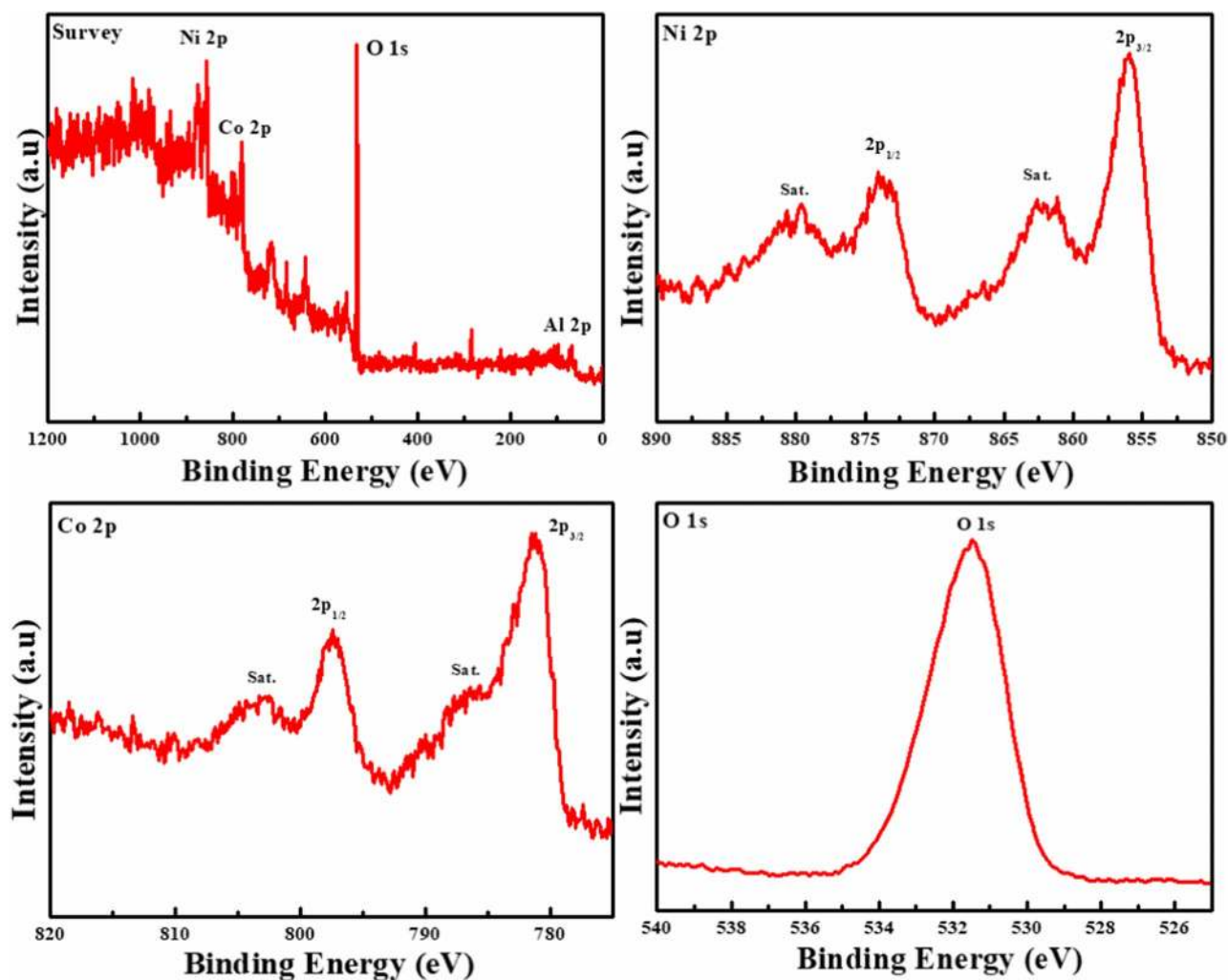

Figure 4. XPS spectra of the sample: (a) the survey spectra, (b)-(d) core level spectra of the Ni 2p, Co 2p and O 1s region, respectively.
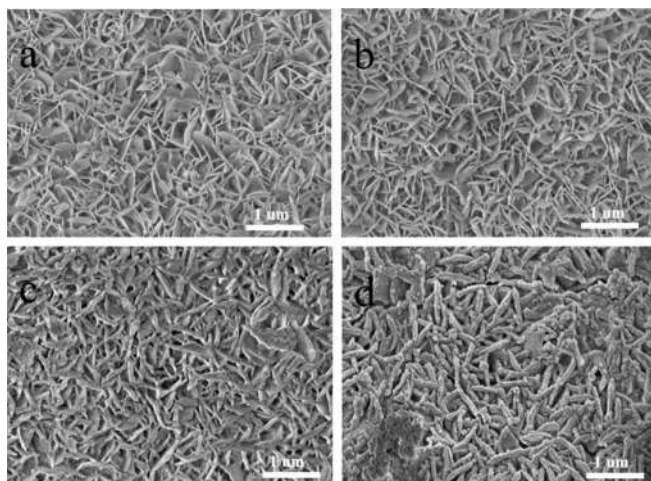
Figure 5. The SEM images (a), (b), (c), (d) of CoAl-LDH@Ni(OH)$_2$ were obtained by electrodeposition at 4 cycles, 6 cycles, 8 cycles, and 10 cycles, respectively.

ferent number of cycles. As shown in Fig. 6, not only the structure of CoAl-LDH preserved its shape even after electrodeposition, but also completely retains the CoAl-LDH@Ni(OH)$_2$ layered structure characteristics. After electrodeposition, the thickness of one single nanoplatelet increases to about 200 nm (8 cycles). The electrochemical deposition of Ni(OH)$_2$ is provided a highly porous structure that the structure increased the contact surface area between active materials and electrolyte.

The elemental distribution of CoAl-LDH@Ni(OH)$_2$ was confirmed by energy dispersive spectroscopy (EDS). Fig. 6c presents the quantitative analysis of the composites of 39.83 wt% Ni, 8.05 wt% Co, 5.54 wt% Al, 31.04 wt% O in the CoAl-LDH@Ni(OH)$_2$-C3 electrode. To further prove the existence of elements in the mixture electrode, the contrast image of the EDS analysis is shown in Figs. 7a–7d. Figs. 7b, 7c, 7d, and 7e show the EDS mapping images of the Ni, Co, O and Al elements from the sample demonstrated in Fig. 7a. Fig. 7 illustrates the chemical component and spatial distribution of the element (Ni, Co, O, Al) in the CoAl-LDH@Ni(OH)$_2$-C3 structure, which demonstrates that the sample is a composite.

showed the peak at 531 eV can be related to hydroxyl ions, suggesting the existence of CoAl-LDH and Ni(OH)$_2$ in the composite.

Figures 5a–5d present the SEM images of CoAl-LDH@Ni(OH)$_2$ attained through electrodeposition at different cycles comprising 4, 6, 8, and 10 cycles, respectively. The CoAl-LDH@Ni(OH)$_2$ composite, as can be seen to contain many curly Ni(OH)$_2$ sheets grown on the surface of the LDH and interlaced with each other forming a 3D porous structure distributed over the entire composite domain. The Ni(OH)$_2$ shell was observed to have different morphology at dif-

Electrochemical evaluation.—Through electrochemical testing, the electrochemical properties of the electrodes were investigated to assess the capability of electrodes in supercapacitors. Figures 8a–8d present the characteristic CV curves of the CoAl-LDH@Ni(OH)$_2$ electrode at diverse scan rates from 5 mVs^{-1} to 100 mVs^{-1}. The cyclic voltammograms of the composites with different cycles were plotted at 5 mV/s, 10 mV/s, 30 mV/s, 50 mV/s, 70 mV/s, and 100 mV/s scanning rates. As the scanning rate increases from 5 mV/s to 100 mV/s, the current response of the four samples increases continuously and the corresponding reduction and oxidation peaks move in the negative and positive directions, respectively. This causesing a continuous surge in
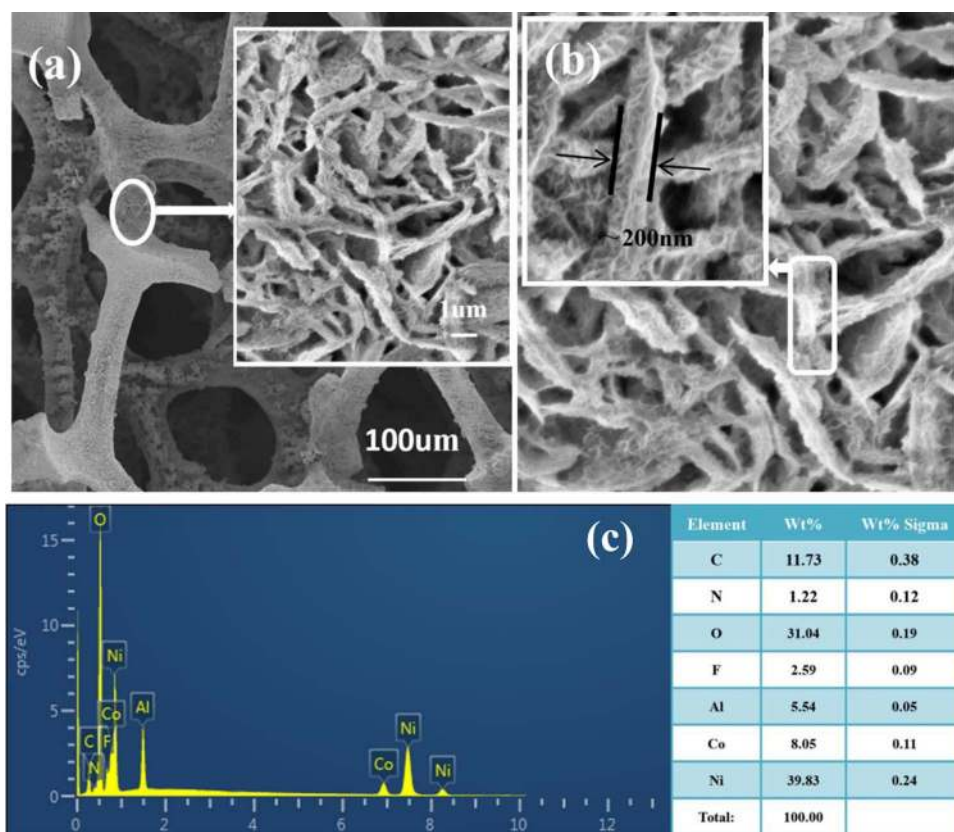

Figure 6. (a) and (b) The SEM images of CoAl-LDH@Ni(OH)$_2$ were obtained by electrodeposition at 8 cycles at different magnification and (c) Quantitative analysis of EDS in large scope.
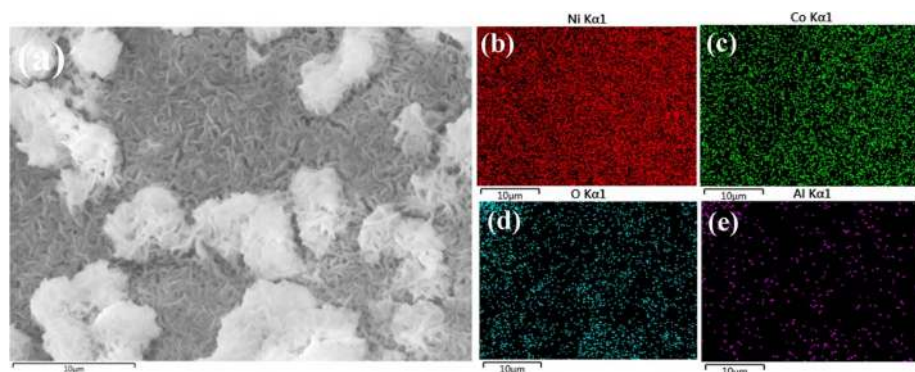
Figure 7. (a) SEM image of the CoAl-LDH@Ni(OH)2-C3 composite, the EDS mapping of (b) Ni, (c) Co, (d) O, and (e) Al.
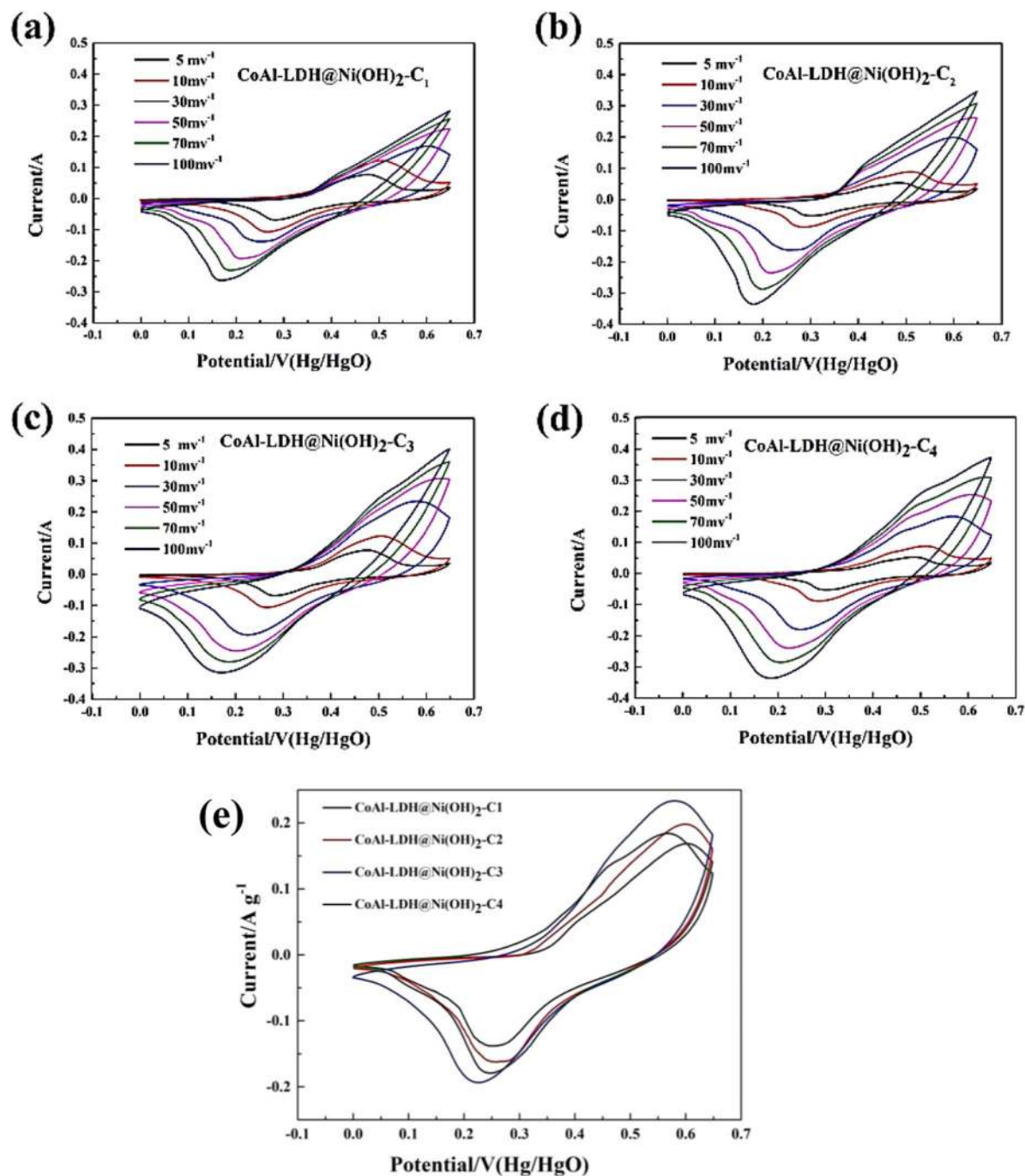

Figure 8. (a-d) Cyclic voltammograms of CoAl-LDH@Ni(OH)$_2$ were obtained by electrodeposition different number of cycles in 6-M KOH aqueous solution, respectively and (e) in 6-M KOH aqueous solution at 30 mV.
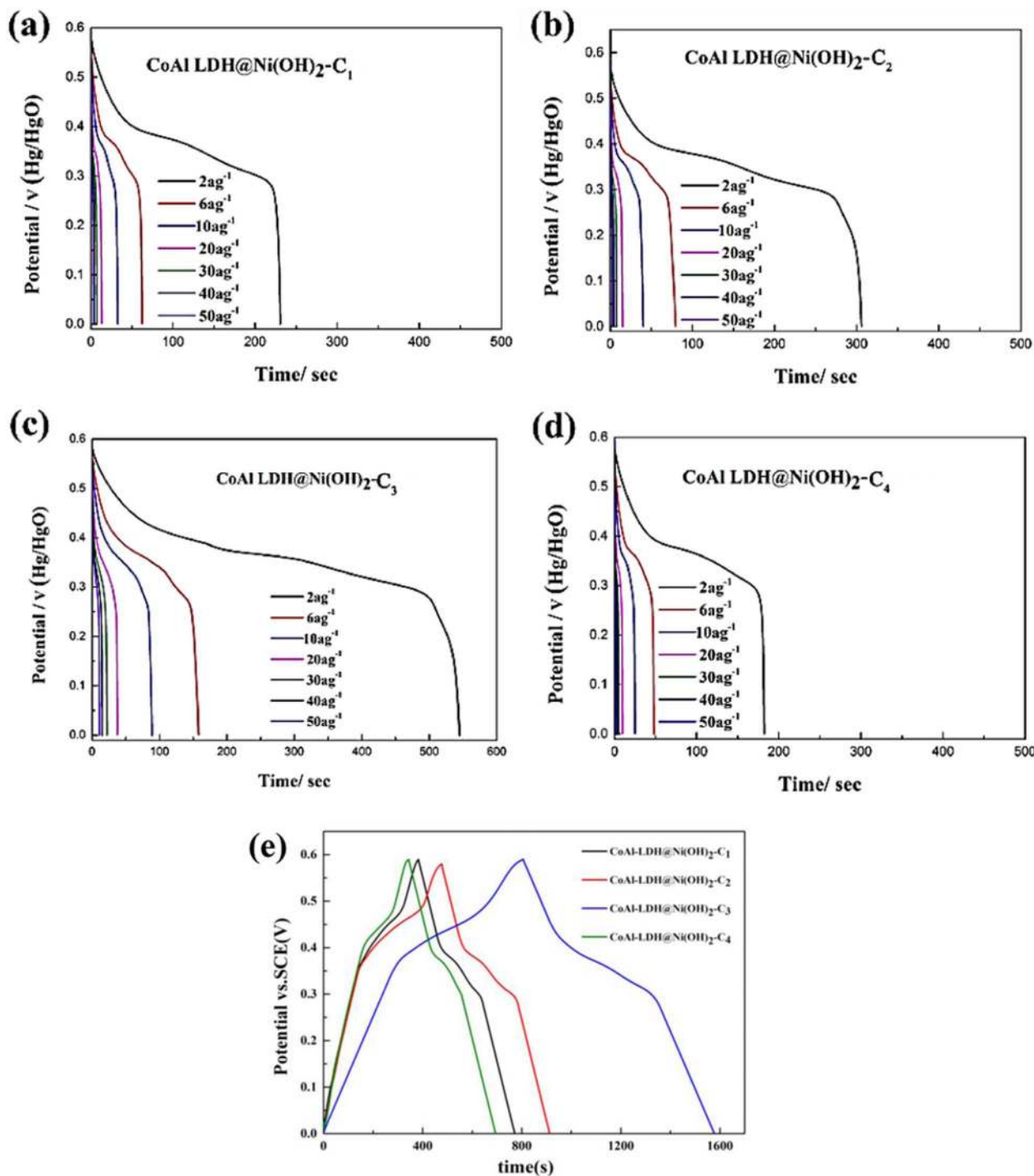
Figure 9. (a-d) Charge/discharge curves CoAl-LDH@Ni(OH)$_2$-C$_1$, CoAl-LDH@Ni(OH)$_2$-C$_2$, CoAl-LDH@Ni(OH)$_2$-C$_3$, and CoAl-LDH @Ni(OH)$_2$-C$_4$ at current densities of 2, 6, 10, 20, 30, 40, and 50 A•g^{-1} in 6-M KOH aqueous solution. (e) Charge/discharge curves of the comparison of the CoAl-LDH@Ni(OH)$_2$ electrodes with different electrodeposited cycles at 2 A g^{-1}.

the potential distance between the reduction and oxidation peaks that specified the redox couples' quasi-reversible feature.[16]

Figure 8e shows the CV of CoAl-LDH@Ni(OH)$_2$ composite with different cycles electrodeposited at a scanning rate of 5 mV · s^{-1}. The potential scanning range is 0~0.65 V (vs. SCE). It is obvious that the integral area of the CV curve of CoAl-LDH@Ni(OH)$_2$ is different, and the shape of the CV curves generated by different electrodeposition cycles are very similar. As shown in Figure 8e, the electrodeposited sample after 8 cycles shows a better charge transfer than other electrodeposited samples after 4, 6, and 10 cycles. The potential change

(ΔEa,c) between the cathodic and anodic peaks of the electrode was utilized as a measure of the electrochemical redox reaction reversibility (i.e., the smaller the ΔEa,c, the higher the reversibility).[15]

The electrode properties of CoAl-LDH@Ni(OH)$_2$ were also tested using galvanostatic charge/discharge measurements. Figures 9a–9d shows the as-prepared composites galvanostatic charge/discharge measurements that were performed in a 6-M KOH aqueous solution in the potential range of 0 to 0.6 V at diverse current densities. It is clear that the charge/discharge curves are nonlinear, confirming the pseudo-capacitive performance of the samples owing to quasi-reversible redox
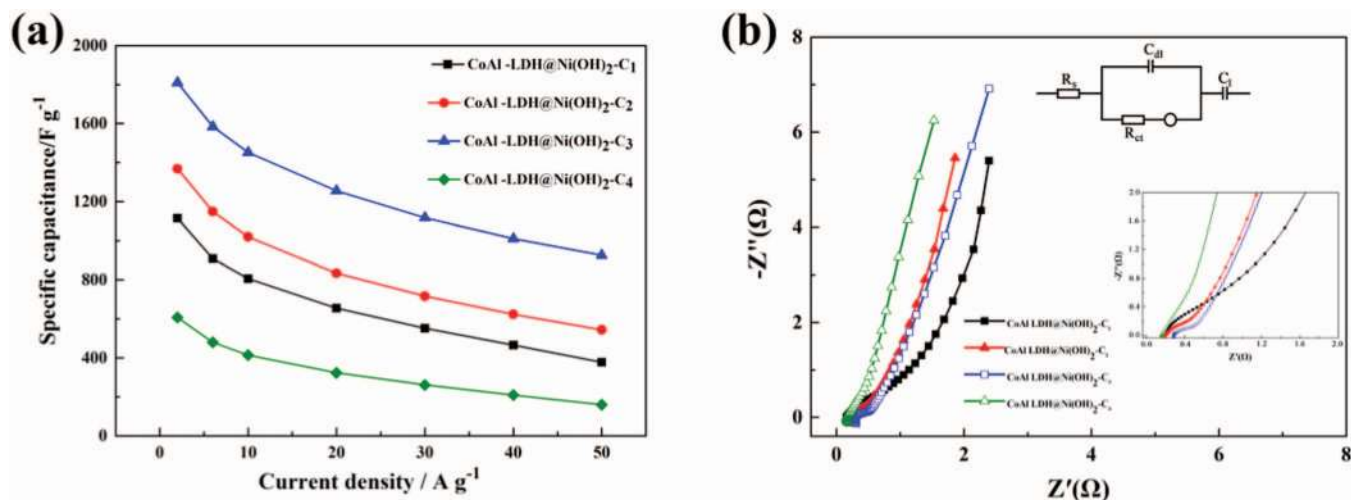
Figure 10. (a) Specific capacitance of the CoAl-LDH@Ni(OH)$_2$ electrodes with different electrodeposited cycles, and (b) Nyquist plots of the CoAl-LDH@Ni(OH)$_2$ electrodes.

reactions at the electrode–electrolyte interface. As depicted in Fig. 9e, the CoAl-LDH@Ni(OH)$_2$-C$_3$ electrodes display a longer discharge time than CoAl-LDH@Ni(OH)$_2$-C$_1$, CoAl-LDH@Ni(OH)$_2$-C$_2$, and CoAl-LDH@Ni(OH)$_2$-C$_4$, at the same current density which suggests a better charge storage performance of the CoAl-LDH@Ni(OH)$_2$-C$_3$ electrodes.[26,28]

According to the Eq. 9, the Coulombic efficiencies of CoAl-LDH@Ni(OH)2-C1, CoAl-LDH@Ni(OH)2-C2, CoAl-LDH@Ni(OH)2-C3, and CoAl-LDH@Ni(OH)2-C4 are 80.41%, 90.14%, 93.37% and 89.77% at 2 A g^{-1}, respectively, which further indicating the best property of the CoAl-LDH@Ni(OH)2-C3.

$$C_e = (CD/CC) \times 100 \qquad [9]$$

where Ce, CD, and CC are Coulombic efficiency, capacity discharged, and capacity charged, respectively.

The samples' specific capacitance (C$_s$) was calculated using the following equation:

$$C_s = \frac{\int I dV}{vmV}$$

where C$_s$, I, Δt, m, v and V are the specific capacity (F/g), the discharge current (A), the discharge time (s), the electrode active material mass (g), the potential scan rate (mV s^{-1}) and the discharge potential interval (V), respectively. Fig. 10a shows that the specific capacity of the electrode material is gradually decreased as the discharge current density increases from 2 A/g to 50 A/g. At the lower current density, all active surface areas of the electrode material can be in good contact with the electrolyte, and a more complete redox reaction occurs with a higher specific capacity. In the larger current density, electrolysis liquid ions and electrode active surface cannot provide an effective contact, eventually leading to a lower specific capacity.

The specific capacitance values of the CoAl-LDH@Ni(OH)$_2$-C3 sample at current densities of 2, 6, 10, 20, 30, 40, and 50 Ag^{-1} are found to be 1810.5, 1584.4, 1451.7, 1255.6, 1117.5, 1010.1, and 926.2 F·g^{-1}, respectively, which shows a better electrochemical performance than other samples, and the specific capacity at 2 A/g reached 1810.55 F/g, maintaining a good capacity retention.[26,28]

To determine the ion transport properties of electrode materials for supercapacitor applications, electrochemical impedance spectroscopy (EIS) tests were investigated over frequency ranges of 0.01 Hz to 100 kHz. Nyquist plots of different mixture electrodes are shown in Fig. 10b, and the proposed equivalent circuit shown in Fig. 10b (inset) is the measured impedance. At low frequency, the equivalent series resistance (E$_{SR}$) of the CoAl-LDH@Ni(OH)$_2$-C4 (0.21 Ω) was smaller than other samples. The EIS result indicates that the LDH nanostructures have a high electrochemical capacity because of their

quick and reversible redox reactions. The Ni(OH)$_2$ materials deposited on the LDH surface and the direct contact with electrolyte indicate the Ni(OH)$_2$ materials have effective reduction in the resistance and lead to fast contact of the electrolyte ions with the surface of the electrode materials.

Figure 11 shows the cycle stability of pure CoAl-LDH electrode and CoAl-LDH@Ni(OH)$_2$ electrodes with different electrodeposited cycles according to the GCD technique at 30 Ag^{-1} for 3000 cycles. The initial increase in specific capacity is due to the activation of active material during the initial cycles.[29] The electrode CoAl-LDH@Ni(OH)$_2$-C$_3$ shows a slow decrease at 2000 cycles and capacitance retention remained at approximately 91% at 1000 cycles and 76% at 3000 cycles. Meanwhile, the capacitance of the pure LDH electrode remained at 65% and 53% at 1000 cycles and 3000 cycles, respectively. It clearly demonstrates that the composite electrodes exhibit excellent cycle stability performance and higher current density.[30]

To further demonstrate the superior capacitive performance of the CoAl-LDH@ Ni(OH)$_2$ on the nickel foam, an asymmetric supercapacitor device was assembled using the CoAl-LDH@Ni(OH)$_2$@NF and MWCNT@NF as positive and negative electrodes, respectively. And the prefabricated PVA/KOH gel electrolyte was placed between positive and negative electrodes as a separator (Fig. 12a). Figure 12b shows the CV curves of MWCNT electrode and CoAl-LDH@Ni(OH)$_2$
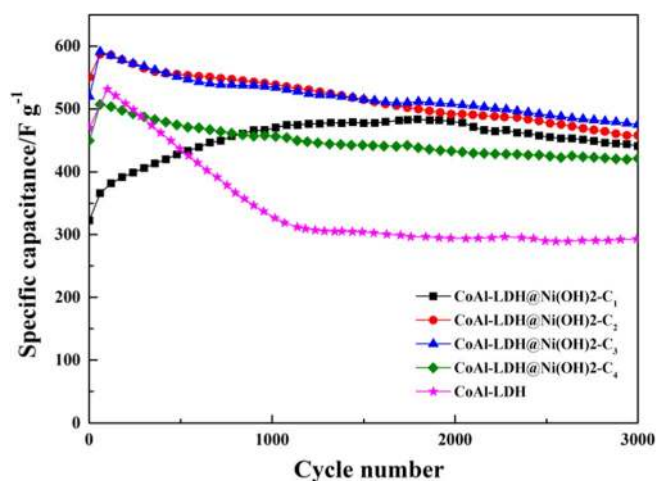

Figure 11. Cycle stability of the CoAl-LDH@Ni(OH)$_2$ electrodes and pure Co-Al-LDH electrode at 30 A g^{-1} for 3000 cycles.
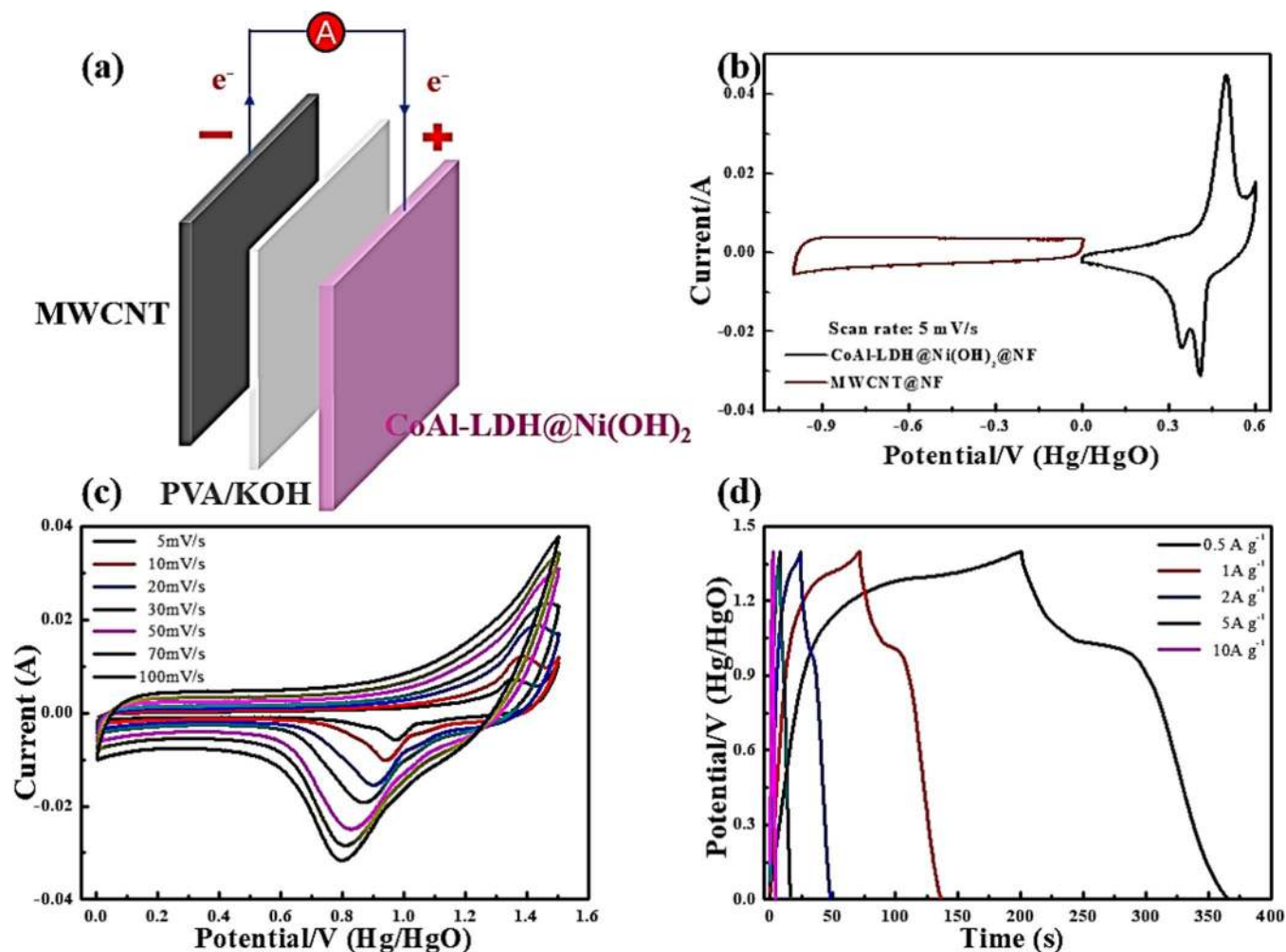
Figure 12. (a) Schematic illustration of the SASC device, (b) CV curves of MWCNT and CoAl-LDH@Ni(OH)$_2$ electrode in three-electrode system at scan rate of 5 mV^{-1}, (c) CV curves of SASC device at different scan rates, (d) Charge-discharge curves at different current densities.

electrode at a scan rate of 5 mV s-1 in a three-electrode test system. The CV curves show that MWCNT (0 ∼ −1 V) and CoAl-LDH@Ni(OH)$_2$ (0 ∼ 0.6 V) electrodes have different potential windows, if they are combined, the potential range of the CoAl-LDH@Ni(OH)$_2$ //MWCNT SASC device can be extended as much as possible, which is beneficial for improving the electrochemical performance of SASC device.

Figure 12c presents the CV curves of SASC at different scan rate between 0–1.6 V, which deviates from a rectangular shape because of the charge storage mechanism of LDH. With the increase in scan rate from 5 mV^{-1} to 100 mV^{-1}, the shape of the CV curves did not change, thereby implying good rapid charge-discharge properties of the device. Figure 12d shows the GCD curves of the asymmetric supercapacitor at various current densities. The energy density (E) and power density (P) values were obtained by the following equations based on the discharge curves:

$$E = \frac{1}{2}CV^2$$

$$P = \frac{E}{\Delta t}$$

where E (Wh kg^{-1}) is the energy density, V (V) is the voltage range excluding the IR drop, P (W kg^{-1}) is the average power density, and Δt is the discharge time.

Based on the specific capacity value, the energy density of the CoAl-LDH@Ni(OH)$_2$ //MWCNT is calculated to 16.72, 12.64, 9.18 and 7.79 Wh kg^{-1} at the power density of 350.01, 702.36, 1399.89 and 3498.87 W kg^{-1}.

The outstanding electrochemical properties of the CoAl-LDH@Ni(OH)$_2$//MWCNT solid-state asymmetric supercapacitor are attributed to the following conditions: 1) the CoAl-LDH@Ni(OH)$_2$ nanoflake structure improves the interfacial contact between the active material and the electrolyte, leading to more efficient charge transportation; 2) the MWCNT@NF negative electrode improves electrolyte accessibility and effective ion-transport pathways, resulting in lower ion-transport resistance; 3) the binder-free electrode reduces internal resistance to ensure fast electrode-electrolyte charge transfer.

Conclusions

In conclusion, we succeeded in growing a new non-binder electrode with a 3D lamellar structure of CoAl-LDH@Ni(OH)$_2$ on a nickel mesh by hydrothermal and electrodeposition techniques. The CoAl-LDH@Ni(OH)$_2$-C$_3$ has excellent electrochemical properties attributed to the increase in the contact area between the active material and the electrolyte by electrodeposition on the surface of the LDH, improving the high conductivity and transfer rate. In addition, the unique layered structure has good conductivity, and suitable mesopore distribution, which improves the faradaic redox reaction and greatly enhances the electrochemical performance.[31] The

experimental results show that the specific capacity is 1810.5 $F \cdot g^{-1}$ at 2 A/g current density and the cycle stability remained at 76% at 30 A g^{-1} for 3000 cycles. Besides, a solid-state asymmetric supercapacitor device was fabricated using CoAl-LDH@Ni(OH)$_2$@NF as the positive electrode and CoAl-LDH@Ni(OH)$_2$@NF as the negative electrode, which achieved high energy and power densities (16.72 Wh kg^{-1} at the power density of 350.01 W kg^{-1}). The results show that the composite electrode material prepared by electrodeposition has great potential in the application of energy storage equipment.

ORCID

Hui Li https://orcid.org/0000-0002-0402-1760
Erfan Zalnezhad https://orcid.org/0000-0002-6878-0352

References

1. A. G. Pandolfo and A. F. Hollenkamp, *J Power Sources*, **157**, 11 (2006).
2. Y. W. Zhu, S. Murali, M. D. Stoller, K. J. Ganesh, W. W. Cai, P. J. Ferreira, A. Pirkle, R. M. Wallace, K. A. Cychosz, M. Thommes, D. Su, E. A. Stach, and R. S. Ruoff, *Science*, **332**, 1537 (2011).
3. X. W. Mao, T. A. Hatton, and G. C. Rutledge, *Curr Org Chem*, **17**, 1390 (2013).
4. F. Stoeckli and T. A. Centeno, *J Mater Chem A*, **1**, 6865 (2013).
5. X. H. Wu, X. T. Hong, Z. P. Luo, K. S. Hui, H. Y. Chen, J. W. Wu, K. N. Hui, L. S. Li, J. M. Nan, and Q. Y. Zhang, *Electrochim Acta*, **89**, 400 (2013).
6. P. Simon and Y. Gogotsi, *Nat Mater*, **7**, 845 (2008).
7. S. Li and C. A. Wang, *J Colloid Interf Sci*, **438**, 61 (2015).
8. C. Z. Yuan, B. Gao, L. F. Shen, S. D. Yang, L. Hao, X. J. Lu, F. Zhang, L. J. Zhang, and X. G. Zhang, *Nanoscale*, **3**, 529 (2011).
9. A. Allagui, T. J. Freeborn, A. S. Elwakil, and B. J. Maundy, *Scientific reports*, **6**, 38568 (2016).
10. J. A. Gursky, S. D. Blough, C. Luna, C. Gomez, A. N. Luevano, and E. A. Gardner, *J Am Chem Soc*, **128**, 8376 (2006).
11. X. J. Pang, L. Chen, Y. Liu, M. J. Chi, Z. F. Li, and J. Plank, *Rsc Adv*, **7**, 14989 (2017).
12. H. Choi and H. Yoon, *Nanomaterials-Basel*, **5**, 906 (2015).
13. A. I. Khan and D. O'Hare, *J Mater Chem*, **12**, 3191 (2002).
14. G. R. Williams and D. O'Hare, *J Mater Chem*, **16**, 3065 (2006).
15. L. J. Zhang, K. N. Hui, K. S. Hui, X. Chen, R. Chen, and H. Lee, *Int J Hydrogen Energ*, **41**, 13329 (2016).
16. L. Zhang, K. N. Hui, K. S. Hui, and H. Lee, *J Power Sources*, **318**, 76 (2016).
17. M. Q. Zhao, Q. Zhang, W. Zhang, J. Q. Huang, Y. H. Zhang, D. S. Su, and F. Wei, *J Am Chem Soc*, **132**, 14739 (2010).
18. J. L. Gunjakar, T. W. Kim, H. N. Kim, I. Y. Kim, and S. J. Hwang, *J Am Chem Soc*, **133**, 14998 (2011).
19. S. He, Z. An, M. Wei, D. G. Evans, and X. Duan, *Chemical Communications*, **49**, 5912 (2013).
20. S. Kaneko and M. Ogawa, *Applied Clay Science*, **75–76**, 109 (2013).
21. A. N. Naveen and S. Selladurai, *Electrochim Acta*, **125**, 404 (2014).
22. Z.-Q. Shen, L. Chen, L. Lin, C.-L. Deng, J. Zhao, Y.-Z. Wang, Z.-Q. Shen, L. Chen, L. Lin, C.-L. Deng, J. Zhao, and Y.-Z. Wang, *Industrial & engineering chemistry research*, **52**, 8454 (2013).
23. Y. Wang, W. S. Yang, C. Chen, and D. G. Evans, *J Power Sources*, **184**, 682 (2008).
24. R. J. Lu, X. Xu, J. P. Chang, Y. Zhu, S. L. Xu, and F. Z. Zhang, *Appl Catal B-Environ*, **111**, 389 (2012).
25. X. X. Guo, F. Z. Zhang, D. G. Evans, and X. Duan, *Chem Commun*, **46**, 5197 (2010).
26. W. Hu, R. Q. Chen, W. Xie, L. L. Zou, N. Qin, and D. H. Bao, *Acs Appl Mater Inter*, **6**, 19318 (2014).
27. Z. Y. Lu, W. Zhu, X. D. Lei, G. R. Williams, D. O'Hare, Z. Chang, X. M. Sun, and X. Duan, *Nanoscale*, **4**, 3640 (2012).
28. S. X. Wu, K. S. Hui, K. N. Hui, and K. H. Kim, *Acs Appl Mater Inter*, **9**, 1395 (2017).
29. T. T. Li, Y. P. Zuo, X. M. Lei, N. Li, J. W. Liu, and H. Y. Han, *J Mater Chem A*, **4**, 8029 (2016).
30. S. Wu, K. S. Hui, K. N. Hui, and K. H. Kim, *J Mater Chem A*, **4**, 9700 (2016).
31. J. B. Han, Y. B. Dou, J. W. Zhao, M. Wei, D. G. Evans, and X. Duan, *Small*, **9**, 98 (2013).
32. H. Li, F. Musharavati, E. Zalenezhad, X. Chen, K. Hui, and K. Hui, *Electrochimica Acta*, **261**, 178 (2017).